Almagro, A., Flores, O., Vera, M., Liñán, A., Sánchez, A. & Williams, F. (2019). Effects of differential diffusion on nonpremixed-flame temperature. *Proceedings of the Combustion Institute, 37*(2), 1757–1766.

DOI: 10.1016/j.proci.2018.06.176

ARTICLE IN PRESS
JID: PROCI [m;October 10, 2018;5:57]

Available online at www.sciencedirect.com

ScienceDirect

Proceedings of the Combustion Institute 000 (2018) 1–10

Proceedings of the Combustion Institute

www.elsevier.com/locate/proci

Effects of differential diffusion on nonpremixed-flame temperature

A. Almagro [a], O. Flores [a], M. Vera [b], A. Liñán [c], A.L. Sánchez [d,*], F.A. Williams [d]

[a] *Dept. Ing. Aeroespacial, Universidad Carlos III de Madrid, Leganés, Spain*
[b] *Dept. Ing. Térmica y de Fluidos, Universidad Carlos III de Madrid, Leganés, Spain*
[c] *E. T. S. I. Aeronáuticos, Pl. Cardenal Cisneros 3, Madrid 28040, Spain*
[d] *Department of Mechanical and Aerospace Engineering, University of California San Diego, La Jolla, USA*

Received 27 November 2017; accepted 22 June 2018
Available online xxx

Abstract

This numerical and analytical study investigates effects of differential diffusion on nonpremixed-flame temperatures. To focus more directly on transport effects the work considers a single irreversible reaction with an infinitely fast rate, with Schab–Zel'dovich coupling functions introduced to write the conservation equations of energy and reactants in a chemistry-free form accounting for non-unity values of the fuel Lewis number L_F. Different flow configurations of increasing complexity are analyzed, beginning with canonical flamelet models that are reducible to ordinary differential equations, for which the variation of the flame temperature with fuel-feed dilution and L_F is quantified, revealing larger departures from adiabatic values in dilute configurations with oxidizer-to-fuel stoichiometric ratios S of order unity. Marble's problem of an unsteady flame wrapped by a line vortex is considered next, with specific attention given to large-Peclet-number solutions. Unexpected effects of differential diffusion are encountered for $S < 1$ near the vortex core, including superadiabatic/subadibatic flame temperatures occurring for values of L_F larger/smaller than unity as well as temperature profiles peaking on the oxidizer side of the flame. Direct numerical simulations of diffusion flames in a temporal turbulent mixing layer are used to further investigate these unexpected differential–diffusion effects. The results, confirming and extending previous findings, underscore the nontrivial role of differential diffusion in nonpremixed–combustion systems.

Keywords: Diffusion flames; Differential diffusion; Vortex flames; Turbulent mixing layer

1. Introduction

Differential-diffusion effects are known to influence critically different properties of nonpremixed flames [1,2], including most notably their temperature, which plays a dominant role in flame

* Corresponding author.
E-mail address: als@ucsd.edu (A.L. Sánchez).

https://doi.org/10.1016/j.proci.2018.06.176
1540-7489 © 2018 The Combustion Institute. Published by Elsevier Inc. All rights reserved.

extinction [3] and may differ notably from the adiabatic-flame value when the Lewis numbers of the reactants are different from unity. The present numerical and analytical investigation is intended to increase understanding of these influences, which are important for developing more accurate models for turbulent combustion [4]. Most previous numerical studies of differential diffusion in nonpremixed flames are based on computations employing finite-rate chemistry (see, e.g., [5] and references therein). Instead, the present work considers the limit of infinitely fast chemistry to uncouple direct effects of differential diffusion on flame temperature from secondary effects arising as a consequence of finite-rate kinetics.

When the fuel-oxidation reactions are sufficiently fast, nonpremixed combustion processes are known to be controlled by the transport rates of the chemical species and heat [6]. The solution can be described in the first approximation by considering the Burke–Schumann (BS) limit of infinitely fast reaction rate, in which the flame appears as a surface separating two equilibrium regions, one without fuel and the other without oxidizer, with the reactants reaching the flame from opposite sides in stoichiometric proportions. In this limit, at any given location the temperature T_f at the flame depends on the transport rates of heat and reactants in the outer equilibrium regions.

To focus on differential-diffusion effects our analysis below will consider radiation-free systems with adiabatic walls. Under those conditions it is well known that, when the reactant diffusivities are equal to the thermal diffusivity (i.e. for unity Lewis numbers of the reactants), the transport rates of reactants and heat are balanced outside the flame in such a way that the resulting BS flame temperature is everywhere equal to the adiabatic flame temperature T_S obtained by burning at constant pressure the reactive mixture formed by mixing the fuel and the oxidizer streams in stoichiometric proportions [2]. In most combustion systems employing air as oxidizer, the assumption of unity Lewis number is a good approximation for O_2. By way of contrast, the fuel Lewis number L_F differs significantly from unity in most cases, the only exceptions being methane and methanol, for which the resulting diffusion-flame temperature T_f differs by a small amount from T_S. For most other fuel-air flames differential-diffusion effects associated with non-unity values of L_F can be expected to be significant, leading to flame temperatures $T_f \neq T_S$. According to the prevailing understanding, for values of $L_F < 1$, corresponding for instance to hydrogen-air combustion, the rate of fuel transport into the flame sheet is higher than the rate of heat removal, resulting in superadiabatic temperatures $T_f > T_S$, while the opposite is expected to occur for heavy fuels with $L_F > 1$.

The value of T_f may vary along the flame as a consequence of the balance of accumulation, convection, and diffusion in the outer equilibrium regions, so that the result depends on the specific flow conditions, including in particular the flow geometry, the relevant Reynolds number, and the dilution of the feed streams. The present investigation is intended to contribute understanding of these dependences by analyzing, sequentially, relevant flow configurations of increasing complexity.

2. Formulation

We address non-premixed combustion systems in which the fuel and the air are provided by different gaseous feed streams, with dilution by addition of an inert gas permitted in the fuel-feed stream for generality. The subscripts A and 0 will be used to denote properties in the air and fuel streams, respectively, so that, for instance, T_A and T_0 are the temperature in the air and fuel feed streams while $Y_{O_2A} = 0.232$ and $Y_{F_0} \leq 1$ are the corresponding reactant mass fractions. The reaction between the fuel and the oxygen is modeled with an infinitely fast irreversible reaction $F + sO_2 \rightarrow (1+s)P + Q$, where s is the mass of oxygen needed to burn the unit mass of fuel. and Q is the amount of heat released in the process. The flame appears as a surface $\Sigma_f(\mathbf{x}, t) = 0$ separating a region without oxygen from a region without fuel. Following [2,3], the problem is formulated with use made of Shvab–Zel'dovich coupling functions, including the two mixture-fraction variables

$$Z = \frac{S\hat{Y}_F - \hat{Y}_O + 1}{S+1} \quad \text{and} \quad \tilde{Z} = \frac{S\hat{Y}_F/L_F - \hat{Y}_O + 1}{S/L_F + 1} \tag{1}$$

and the normalized enthalpy variable

$$\xi = \frac{(T - T_A)/T_A + (q/S)(\hat{Y}_O - 1)}{(T_0 - T_A)/T_A - q/S}, \tag{2}$$

involving the the normalized reactant mass fractions $\hat{Y}_O = Y_{O_2}/Y_{O_2A}$ and $\hat{Y}_F = Y_F/Y_{F_0}$, the temperature T, the mass of air needed to burn the unit mass of the fuel stream $S = sY_{F_0}/Y_{O_2A}$, and the dimensionless temperature increase $q = (QY_{F_0})/(c_pT_A)$, with c_p denoting the specific heat at constant pressure, assumed to be constant. The coupling functions satisfy the conservation equations

$$\frac{\partial}{\partial t}(\rho Z) + \nabla\cdot(\rho\mathbf{v}Z) - \frac{1}{L_m}\nabla\cdot\left(\rho D_T\nabla\tilde{Z}\right) = 0, \tag{3}$$

involving the effective Lewis number $L_m = (S+1)/(S/L_F+1)$, and

$$\frac{\partial}{\partial t}(\rho\xi) + \nabla\cdot(\rho\mathbf{v}\xi) - \nabla\cdot(\rho D_T\nabla\xi) = 0, \tag{4}$$

with boundary conditions $Z = \tilde{Z} = \xi = 1$ in the fuel stream and $Z = \tilde{Z} = \xi = 0$ in the air stream. In the notation, ρ and D_T represent the density and the thermal diffusivity, respectively. At the flame surface $\Sigma_f(\mathbf{x}, t) = 0$ the reactant mass fractions $\hat{Y}_F$

Please cite this article as: A. Almagro et al., Effects of differential diffusion on nonpremixed-flame temperature, Proceedings of the Combustion Institute (2018), https://doi.org/10.1016/j.proci.2018.06.176

and $\hat{Y}_O$ are simultaneously zero, corresponding to values of the mixture fraction variables $Z = Z_S$ and $\tilde{Z} = \tilde{Z}_S$, with

$$Z_S = \frac{1}{S+1} \quad \text{and} \quad \tilde{Z}_S = \frac{1}{S/L_F + 1}. \tag{5}$$

The chemical–equilibrium condition $\hat{Y}_O \hat{Y}_F = 0$ together with the definitions (1) and (2) provide piecewise linear relations for the composition

$$\begin{cases} \hat{Y}_O = 0, \ \hat{Y}_F = \frac{Z - Z_S}{1 - Z_S} = \frac{\tilde{Z} - \tilde{Z}_S}{1 - \tilde{Z}_S} & \text{for } Z \geq Z_S \\ \hat{Y}_F = 0, \ \hat{Y}_O = 1 - \frac{Z}{Z_S} = 1 - \frac{\tilde{Z}}{\tilde{Z}_S} & \text{for } Z \leq Z_S \end{cases} \tag{6}$$

and temperature

$$\begin{cases} \frac{T}{T_A} - 1 = \frac{T_0 - T_A}{T_A}\xi + \frac{q}{S}(1 - \xi) & \text{for } Z \geq Z_S \\ \frac{T}{T_A} - 1 = \frac{T_0 - T_A}{T_A}\xi + \frac{q}{S}\left(\frac{\tilde{Z}}{\tilde{Z}_S} - \xi\right) & \text{for } Z \leq Z_S \end{cases}, \tag{7}$$

the latter involving the ratio q/S, related through

$$\frac{T_S - T_A}{T_A} = \frac{T_0 - T_A}{T_A} Z_S + \frac{q}{S}(1 - Z_S) \tag{8}$$

to the adiabatic flame temperature T_S.

The numerical solution requires in general integration of the transport equations (3) and (4) coupled with the continuity and momentum equations. In the integration, the relationships (6) and (7) are employed to evaluate the temperature and composition in terms of Z and ξ, with the equation of state used to compute the density. Additionally, expressions must be provided for the transport properties in terms of the temperature and composition. The distribution of $\xi_f(\mathbf{x}, t)$ on the flame surface $\Sigma_f(\mathbf{x}, t) = 0$, to be obtained as part of the solution, determines the flame temperature T_f according to

$$\frac{T_f - T_A}{T_A} = \frac{T_0 - T_A}{T_A}\xi_f + \frac{q}{S}(1 - \xi_f). \tag{9}$$

The solution simplifies greatly for $L_F = 1$, when $Z = \tilde{Z} = \xi$ everywhere in the flow field. Consequently, the flame value of ξ is simply $\xi_f = Z_S = 1/(S+1)$ and the associated flame temperature evaluated from (9) becomes $T_f = T_S$, equal to the adiabatic flame temperature defined in (8). By way of constrast, when $L_F \neq 1$ the value of ξ_f differs in general from Z_S. Correspondingly, the flame temperature computed from (9) deviates from the stoichiometric adiabatic value by an amount given by

$$\frac{T_f - T_S}{(q/S)T_A + (T_A - T_0)} = Z_S - \xi_f, \tag{10}$$

obtained by subtracting (8) from (9). As can be inferred from (10), since the characteristic temperature increase due to combustion $(q/S)T_A$ is much larger than $T_A - T_0$ for cases of practical interest, values of ξ_f higher/lower than Z_S correspond to subadiabatic/superadiabatic flame temperatures, respectively.

Differential-diffusion effects can be anticipated to be larger in steady flows dominated by diffusive transport, when the solution to (3) and (4) reduces to $\xi = \tilde{Z}$. The associated flame value of the enthalpy variable $\xi_f = \tilde{Z}_S$ can be used in (10) to yield

$$\frac{T_D - T_S}{(q/S)T_A + (T_A - T_0)} = \frac{Z_S(1 - Z_S)(1 - L_F)}{1 - (1 - L_F)Z_S}, \tag{11}$$

where T_D is the flame temperature with diffusion-controlled transport. Although one would expect the flame temperature to lie between the adiabatic stoichiometric value T_S and the diffusion-controlled value T_D given in (11), the computations presented below will reveal more complex behaviors, with the interactions occurring in the outer transport regions leading to flame temperatures lying outside these anticipated bounds.

3. Canonical flamelet models

The simplest solutions to the above transport problem arise in connection with laminar diffusion flames formed in steady counterflow mixing layers and in one-dimensional unsteady mixing layers. As shown in [7], in both cases introduction of an appropriately defined density–weighted dimensionless coordinate η under the assumption of constant $\rho^2 D_T$ (and with the additional approximation of constant strain rate for the counterflow) reduces the problem to the integration of

$$\frac{\tilde{Z}''}{L_m} + \eta Z' = \xi'' + \eta \xi' = 0 \begin{cases} \tilde{Z} = \xi = 0 \text{ at } \eta = -\infty \\ \tilde{Z} = \xi = 1 \text{ at } \eta = \infty \end{cases} \tag{12}$$

supplemented with (6), with the prime denoting differentiation with respect to η. Straightforward integration provides $\xi = \frac{1}{2}\left[1 + \text{erf}(\eta/\sqrt{2})\right]$ for the enthalpy variable, while the expressions for the mixture fraction, different on each side of the flame, are

$$\begin{cases} \frac{\tilde{Z}}{\tilde{Z}_S} = \frac{1 + \text{erf}(\eta/\sqrt{2})}{1 + \text{erf}(\eta_f/\sqrt{2})} & \text{for} \quad \eta \leq \eta_f \\ \frac{\tilde{Z} - \tilde{Z}_S}{1 - \tilde{Z}_S} = 1 - \frac{1 - \text{erf}(\eta\sqrt{L_F/2})}{1 - \text{erf}(\eta_f\sqrt{L_F/2})} & \text{for} \quad \eta \geq \eta_f \end{cases} \tag{13}$$

As shown in [3], the flame location η_f is determined from the implicit equation

$$\left(\frac{S}{\sqrt{L_F}}\right) \frac{\exp(-L_F \eta_f^2/2)}{1 - \text{erf}(\eta_f\sqrt{L_F/2})} = \frac{\exp(-\eta_f^2/2)}{1 + \text{erf}(\eta_f/\sqrt{2})} \tag{14}$$

obtained by imposing the continuity of $\mathrm{d}\tilde{Z}/\mathrm{d}\eta$ at the flame. The value of η_f can be used to yield

$$\xi_f = \frac{1 + \text{erf}(\eta_f/\sqrt{2})}{2}. \tag{15}$$

Please cite this article as: A. Almagro et al., Effects of differential diffusion on nonpremixed-flame temperature, Proceedings of the Combustion Institute (2018), https://doi.org/10.1016/j.proci.2018.06.176

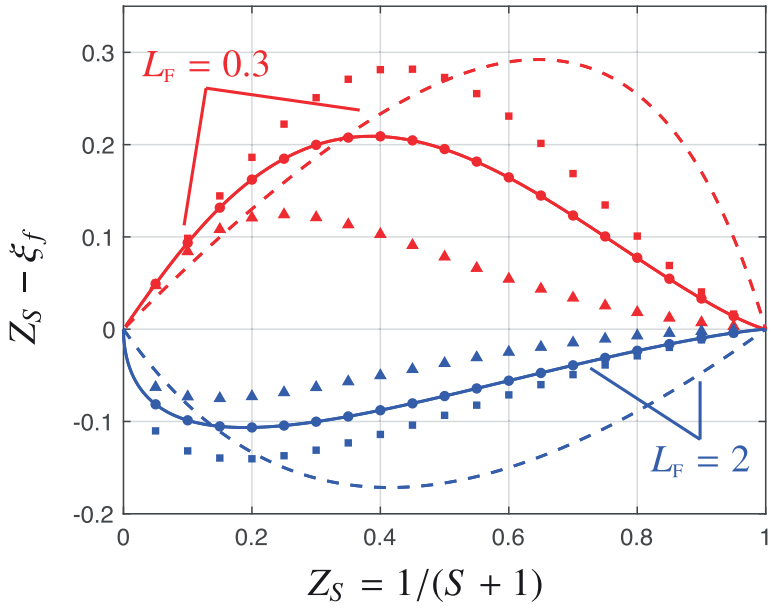

Fig. 1. The dimensionless temperature increase $Z_S - \xi_f$ obtained for the counterflow and unsteady mixing layers (solid curves), for coflow diffusion flames ($U_0/U_A = \infty$ squares; $U_0/U_A = 1$ circles; $U_0/U_A = 0$ triangles), and for diffusion-dominated transport (dashed curves).

Rescaled temperature departures $Z_S - \xi_f$, obtained with use made of (14) and (15) to determine ξ_f, are shown as solid curves in Fig. 1 for $0 \le Z_S \le 1$ and two different fuel Lewis numbers, $L_F = 0.3$ and $L_F = 2.0$, selected to represent the properties of hydrogen and of a heavy hydrocarbon, where they may be compared with the diffusion-dominated dashed curves. As expected, subadiabatic flame temperatures $Z_S - \xi_f < 0$ are found for $L_F = 2.0$, whereas the opposite behavior is found for $L_F = 0.3$. Differential-diffusion effects are more pronounced at intermediate values of Z_S, causing the values of $|Z_S - \xi_f|$ to reach a maximum there. For the small values of Z_S characterizing combustion with air, the observed temperature departures are on the order of 5%, increasing to values on the order of 10% in hydrocarbon-oxygen ($Z_S \simeq 0.2$) and hydrogen-oxygen ($Z_S \simeq 0.11$) systems.

Another configuration that is reducible to ordinary differential equations is the diffusion flame formed in the coflow mixing layer separating two parallel streams of fuel and air with velocities U_0 and U_A. The transport equations obtained in that case by introduction of a density–weighted transverse coordinate with constant $\rho^2 D_T$ are those given above in (12) with the factor η in the convective terms replaced by a selfsimilar stream function $F(\eta)$ satisfying $PrF''' + FF'' = 0$ subject to $F'(-\infty) - 1 = F(0) = F'(\infty) - U_0/U_A = 0$, with $Pr = 0.7$ denoting here the Prandtl number. Resulting values of $Z_S - \xi_f$ are shown in Fig. 1 for the extreme cases of stagnant air ($U_0/U_A = \infty$) and stagnant fuel ($U_0/U_A = 0$). For $U_0/U_A = 1$, we find $F = \eta$, so that the corresponding temperature departure is that of the counterflow. Increasing U_0/U_A results in a larger velocity in the flame region and in flames lying closer to the oxidizer boundary, enhancing differential diffusion effects, as seen in the corresponding values of $Z_S - \xi_f$. The different curves are compared with the temperature increase obtained when transport is dominated by diffusion, given in (11), revealing that the magnitude of the temperature departure from the adiabatic value $|T_f - T_S|$ can be larger than $|T_D - T_S|$ for sufficiently small values of Z_S. This unexpected finding is a first indication of the nontrivial character of differential-diffusion effects. These effects occur for Z_S near zero because the oxygen Lewis number is unity; if it were not but the fuel Lewis number had been unity, then corresponding anomalies would arise instead for Z_S near one.

4. Diffusion flame in a vortex

As an example of a flow that exhibits a spatially varying flame temperature, consider now a diffusion flame distorted by a vortex, a problem addressed by Marble [8] as a model to analyze nonpremixed combustion in turbulent mixing layers; see also [9,10]. The initial condition assumes two semi-infinite spaces of fuel and air separated by an initially planar interface. Mixing and reaction occur as the interface is distorted by the presence

Please cite this article as: A. Almagro et al., Effects of differential diffusion on nonpremixed-flame temperature, Proceedings of the Combustion Institute (2018), https://doi.org/10.1016/j.proci.2018.06.176

of a line vortex of constant circulation Γ located at the interface. In the approximation of constant density and constant transport properties the velocity induced is purely azimuthal, with magnitude $\Gamma/(2\pi r')$ decreasing inversely proportional to the distance r' from the vortex. Because of the absence of geometrical scales there exists a selfsimilar solution involving the rescaled radial coordinate $r = r'/\sqrt{(\Gamma t)/(2\pi)}$, which reduces the problem to that of integrating

$$-\frac{r^3}{2}\frac{\partial Z}{\partial r}+\frac{\partial Z}{\partial \theta}=\frac{1}{Pe}\frac{1}{L_m}\left(r^2\frac{\partial^2 \tilde{Z}}{\partial r^2}+r\frac{\partial \tilde{Z}}{\partial r}+\frac{\partial^2 \tilde{Z}}{\partial \theta^2}\right) \tag{16}$$

$$-\frac{r^3}{2}\frac{\partial \xi}{\partial r}+\frac{\partial \xi}{\partial \theta}=\frac{1}{Pe}\left(r^2\frac{\partial^2 \xi}{\partial r^2}+r\frac{\partial \xi}{\partial r}+\frac{\partial^2 \xi}{\partial \theta^2}\right) \tag{17}$$

for $r \geq 0$ with the condition that all coupling functions be 2π-periodic in θ, regular at $r = 0$, and such that $Z = \tilde{Z} = \xi = 1$ for $0 < \theta < \pi$ and $Z = \tilde{Z} = \xi = 0$ for $0 > \theta > -\pi$ as $r \to \infty$. The solution depends on the stoichiometric parameter S, on the Lewis number L_F, and on the Peclet number $Pe = \Gamma/(2\pi D_T)$[1].

Resulting flame shapes are shown in Fig. 2 for $S = 0.5$, $L_F = 2$, and $Pe = (10, 100, 1000)$ along with the variation with radial distance of the accompanying temperature distributions along the two flame branches as they wrap around the vortex. The far-field solution, with negligible effects of convection, naturally reduces to the one-dimensional unsteady mixing layer described by (12), which can be formally derived from (16) and (17) by introducing $\eta = \sqrt{Pe/2}r\theta$ (or $\eta = \sqrt{Pe/2}r(\pi - \theta)$) before taking the limit $r \to \infty$. Consequently, as shown in the lower plot of Fig. 2, the temperature departure along the vortex flame approaches for $r \to \infty$ the value $Z_S - \xi_f \simeq -0.045$ obtained from (14) and (15) for $S = 0.5$ and $L_F = 2$. The case $S = 0.5$ has been purposely selected to illustrate a surprising aspect of the solution, namely, that for $S < 1$ differential-diffusion effects near the vortex core generate temperature departures that are opposite in sign to those expected. Specifically, for $L_F = 2$ the flame temperature, subadiabatic in the flame wings away from the core, evolve to give superadiabatic temperatures in the core. Although the temperature evolves differently along the two branches, with the temperature along the branch originating at $\theta = \pi$ increasing to higher values, the differences observed decrease drastically for larger values of Pe, a limit to be addressed below.

In the limit $Pe \to \infty$ mixing is confined to thin layers of characteristic thickness $Pe^{-1/2}$ about the spiral interfaces $\theta - r^{-2} = 0$ and $\theta - r^{-2} = \pi$. As shown by Liñán [11], the analysis of this limit is facilitated by introduction of the alternative coordinates

$$\mu = \theta - r^{-2} \quad \text{and} \quad \tau = \frac{1}{Pe}\left(\frac{4}{3r^6}+\frac{1}{r^2}\right) \tag{18}$$

to write (16) and (17) in the form

$$\frac{\partial Z}{\partial \tau}-\frac{1}{L_m}\frac{\partial^2 \tilde{Z}}{\partial \mu^2}=\frac{\partial \xi}{\partial \tau}-\frac{\partial^2 \xi}{\partial \mu^2}=0 \tag{19}$$

after neglecting smaller terms in negative powers of Pe. In this leading-order approximation the solutions along the two spiral branches are identical. The branch originating at $\theta = 0$ is described by integration of (19) with initial conditions

$$\left.\begin{array}{lll} Z=\tilde{Z}=\xi=0 & \text{for} & -\frac{\pi}{2}<\mu<0 \\ Z=\tilde{Z}=\xi=1 & \text{for} & 0<\mu<\frac{\pi}{2} \end{array}\right\} \text{ at } \tau = 0 \tag{20}$$

and boundary conditions

$$\frac{\partial Z}{\partial \mu}=\frac{\partial \tilde{Z}}{\partial \mu}=\frac{\partial \xi}{\partial \mu}=0 \text{ at } \mu=\pm\frac{\pi}{2}, \tag{21}$$

consistent with the periodicity of the solution.

The problem stated in (19)–(21) describes the combustion of adjacent strips of fuel and air wrapped by the vortex, with increasing pseudotimes τ corresponding to decreasing distances from the vortex core. The resulting distributions of $Z(\mu, \tau)$ and $\tilde{Z}(\mu, \tau)$ determine the flame location $\mu = \mu_f(\tau)$ from the condition $\tilde{Z}(\mu_f, \tau) = \tilde{Z}_S$ (or $Z(\mu_f, \tau) = Z_S$). Since $Z \to 1/2$ near the vortex center (i.e. as $\tau \to \infty$) the flame for $S \neq 1$ spirals to reach a finite radius (smaller for smaller values of $|S - 1|$), defined by the last value of τ at which $Z(\mu_f, \tau) = Z_S$. Predicted flame shapes can be expressed in the original coordinates as $\theta = \mu_f(\tau) + r^{-2}$, with τ given in (18) carrying the dependence on Pe. As shown in the comparisons of Fig. 2, the agreement with the results of numerical computations is excellent for $Pe = 100$, and the curves are virtually indistinguishable for $Pe = 1000$.

The temperature changes along the spiral flame, as determined by $\xi_f(\tau) = \xi(\mu_f, \tau)$. As shown in the comparisons of the lower plot of Fig. 2, although the model at this order fails to predict the differences in temperature between the two branches, smaller for larger Pe, the asymptotic prediction describes with sufficient accuracy the temperature evolution as the vortex core is approached.

Additional computations of $Z_S - \xi_f$ in the limit $Pe \gg 1$ are shown in Fig. 3 for different values of S with $L_F = 0.3$ and $L_F = 2$. The values for $\tau \ll 1$, corresponding to large radial distances away the

[1] It is worth noting that the same mathematical problem is encountered for the case of a steady diffusion flame wrapped in a stretched vortex with radial, axial, and azimuthal velocity components $v_r = -Ar'/2$, $v_z = Az$, and $v_\theta = \Gamma/(2\pi r')$, with the corresponding self-similar coordinate being in that case $r = r'/\sqrt{\Gamma/(2\pi A)}$.

Please cite this article as: A. Almagro et al., Effects of differential diffusion on nonpremixed-flame temperature, Proceedings of the Combustion Institute (2018), https://doi.org/10.1016/j.proci.2018.06.176

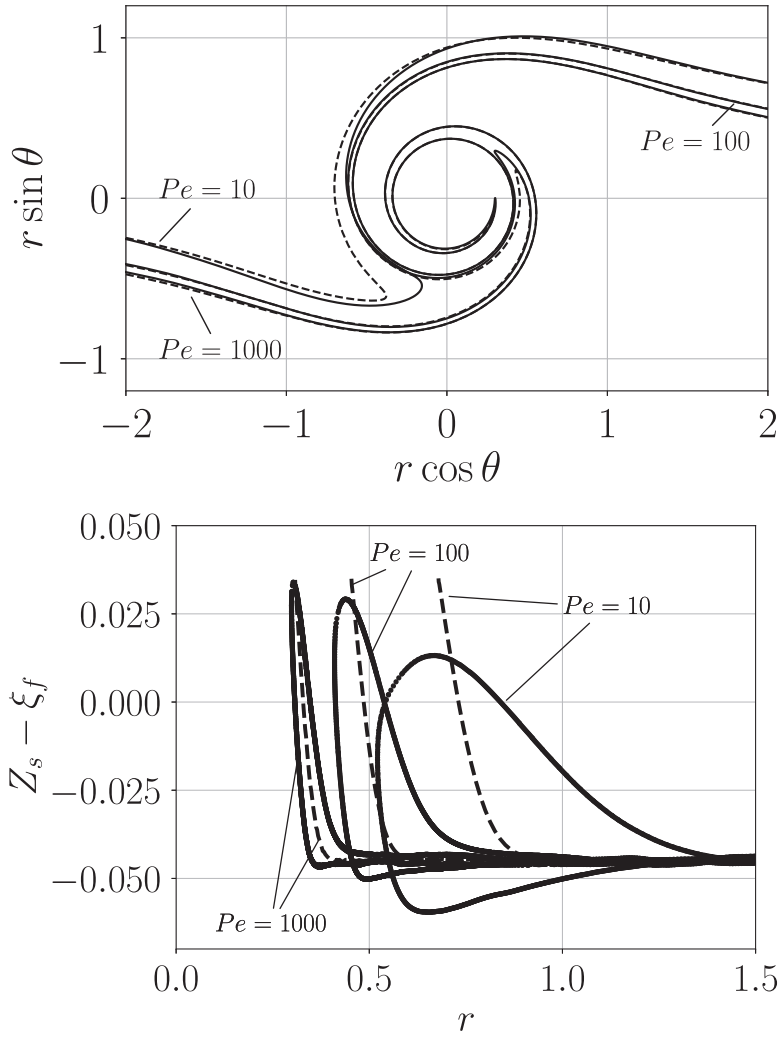

Fig. 2. The solid curves represent isosurfaces $\tilde{Z}(\eta, \theta) = \tilde{Z}_S$ and accompanying temperature distributions obtained from (16) and (17) for $S = 0.5$, $L_F = 2$, and $Pe = (10, 100, 1000)$, while the dashed curves are evaluated from the asymptotic results for $Pe \gg 1$.

vortex core, are those for one-dimensional unsteady mixing-layer flames, represented as solid curves in Fig. 1. The evolution of the temperature as the vortex core is approached (i.e. for increasing τ) is different depending on whether S is larger or smaller than unity, a condition that determines the excess reactant present in the vortex core, as can be seen by comparing the vortex-center value $Z = 1/2$ with the stoichiometric value $Z_S = 1/(S + 1)$. For configurations with $S > 1$, when fuel is the excess reactant in the vortex core, the resulting flame temperature remains superadiabatic everywhere for $L_F = 0.3$ and subadiabatic everywhere for $L_F = 2$, whereas for flames with $S < 1$ the temperature departure $Z_S - \xi_f$ vanishes at an intermediate radius and reverses its sign closer to the vortex center. These unexpected differential-diffusion effects occur during the final stage of fuel depletion, when the flame moves rapidly across the fuel strip, altering the balance of fuel diffusion to and heat removal from the flame. The associated rapid evolution is illustrated in an inset of Fig. 3, which shows temperature profiles obtained for the three radii indicated by the points shown along the curve corresponding to $L_F = 0.3$ and $S = 0.5$. The rapid displacement towards the fuel side places the flame in a region where less oxygen is available, thereby resulting in a decreasing flame temperature. The decrease is so rapid that for $\tau = 0.8$ the maximum temperature is no longer at the flame, but rather it is on

Please cite this article as: A. Almagro et al., Effects of differential diffusion on nonpremixed-flame temperature, Proceedings of the Combustion Institute (2018), https://doi.org/10.1016/j.proci.2018.06.176

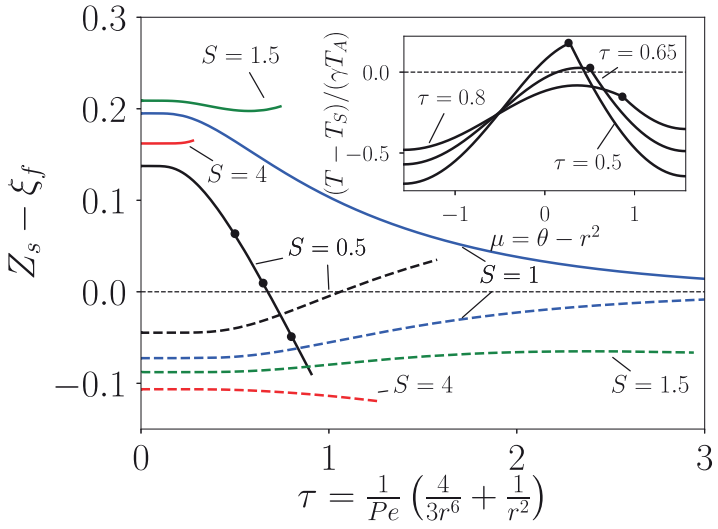

Fig. 3. The variation of the temperature departure $Z_S - \xi_f$ as evaluated in the limit $Pe \gg 1$ for $L_F = 0.3$ (solid curves) and $L_F = 2$ (dashed curves); the inset represents near-flame distributions for $L_F = 0.3$ and $S = 0.5$ for the three radial distances indicated with the circles.

the oxidizer side, corresponding to the hot products generated at an earlier pseudo-time τ (i.e. at larger values of r).

5. Nonpremixed flame evolution in a turbulent mixing layer

We investigate now Burke–Schumann diffusion flames embedded in a three-dimensional, turbulent, low-Mach-number, temporally evolving mixing layer separating a fuel stream from an air stream. This problem was considered earlier for unity Lewis numbers [12,13], with differential-diffusion effects investigated for two-dimensional constant-density flow in [14]. As in these previous investigations, integrations are performed for large values of the Peclet number $Pe = \Delta U \delta / D_{T_A} \sim 10^4$, with ΔU and δ representing the velocity jump across the mixing layer and the initial vorticity thickness. The formulation assumes constant values of the molecular weight and a constant Prandtl number $Pr = 0.7$, but accounts for the temperature variation of the density $\rho \propto T^{-1}$ and transport properties $D_T \propto T^{1.7}$. A variant of the code used earlier in analyzing non-reacting variable-density mixing layers [15] was employed in the integrations (see [16] for details), which were extended until the Reynolds number based on the Taylor scale reached values on the order of $Re_\lambda \simeq 90 - 120$. Sample distributions of $\tilde{Z}$ and T/T_A are shown for $L_F = 0.3$ and $S = 0.5$ in the color contours of Fig. 4, with a solid curve used to represent the location of the flame sheet, given by the isosurface $\tilde{Z} = \tilde{Z}_S$. As can be seen, although the oxidizer-to-fuel ratio S is smaller than one, the flame is slightly displaced towards the air side of the mixing layer as a result of the large fuel diffusivity.

Of particular interest in the present discussion is the resulting distribution of temperature at the flame surface, with representative probability distributions given in Fig. 5 for $L_F = (0.3, 2)$ and $S = (0.5, 1)$. The results agree with those of the vortex-flame model in that, while the flame temperature lies mostly above T_S for $L_F = 0.3$ and below T_S for $L_F = 2.0$, there are areas of the flame surface that display the opposite behavior, with the effect being noticeably more pronounced for $S = 0.5$ and $L_F = 0.3$, when nearly 10% of the flame surface exhibits subadiabatic temperatures.

When the temperature difference $T_A - T_0$ between the two feed streams is not too pronounced, the general expectation is that the peak temperature is always attained at the flame surface. Because of effects of differential diffusion, however, this does not necessarily happen everywhere, as pointed out earlier [14]. For instance, the inset of Fig. 3 displays an illustration of this nonstandard behavior for the Marble problem when the fuel feed is sufficiently dilute, leading to temperatures peaking on the oxidizer side near the vortex core. The extent of this phenomenon in turbulent Burke–Schumann flames can be assessed by computing the rates of heat loss to both sides of the flame surface, which balance the rate of chemical heat release at the flame. The computation, involving (7) to express the temperature in terms of $\tilde{Z}$ and ξ, yields

Please cite this article as: A. Almagro et al., Effects of differential diffusion on nonpremixed-flame temperature, Proceedings of the Combustion Institute (2018), https://doi.org/10.1016/j.proci.2018.06.176

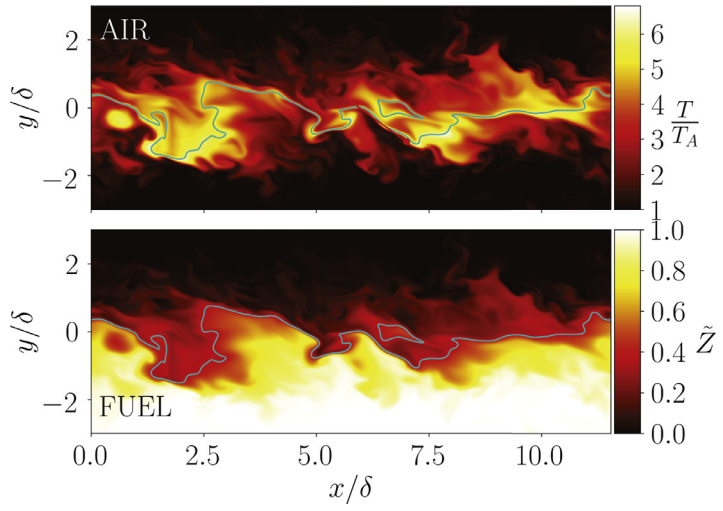

Fig. 4. A transverse cut of the instantaneous distributions of $\tilde{Z}$ and T/T_A for $T_A = T_0$, $L_F = 0.3$, $S = 0.5$, $Pe = 14,280$, and $(q/S) = 1.33$.

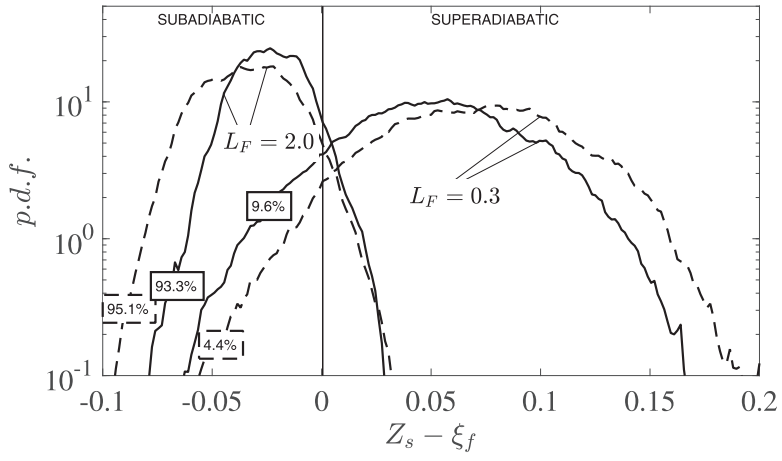

Fig. 5. The probability density distribution of the relative flame-temperature departure for $S = 0.5$ (solid curves) and $S = 1.0$ (dashed curves).

$$\gamma_F = 1 - \gamma_O = \left(1 + \frac{T_A - T_0}{(q/S)T_A}\right) Z_S \left.\frac{\nabla\xi \cdot \nabla\tilde{Z}}{\nabla\tilde{Z} \cdot \nabla\tilde{Z}}\right|_f \tag{22}$$

for the fraction of chemical heat release γ_F that is conducted towards the fuel side of the flame, with γ_O representing the fraction transported to the oxidizer side. When the local peak temperature occurs at the flame, the resulting heat-loss rate on both sides is positive, so that $0 < \gamma_F = 1 - \gamma_O < 1$. Correspondingly, peak temperatures occur on the fuel side when $\gamma_F < 0$ and on the oxidizer side when $\gamma_F > 1$ (i.e. when $\gamma_O < 0$).

The solution simplifies for $L_F = 1$, when $\xi = \tilde{Z}$ everywhere, so that (22) yields the constant value $\gamma_F = [1 + (T_A - T_0)/(qT_A/S)]Z_S$ at every point on the flame surface. For $L_F \neq 1$ the computation of γ_F through (22) requires evaluation of $\nabla\tilde{Z}$ and $\nabla\xi$ at the flame. Resulting probability density functions associated with the turbulent flames of Fig. 5 are shown in Fig. 6. While the peak temperature is seen to occur predominantly at the flame, a nonnegligible fraction of the flame surface displays off-flame peak temperatures. For the cases considered, involving significant fuel-feed dilution (i.e. values of S of order unity), the peak temperature is rarely found on the fuel side, while occurrence of max-

Please cite this article as: A. Almagro et al., Effects of differential diffusion on nonpremixed-flame temperature, Proceedings of the Combustion Institute (2018), https://doi.org/10.1016/j.proci.2018.06.176

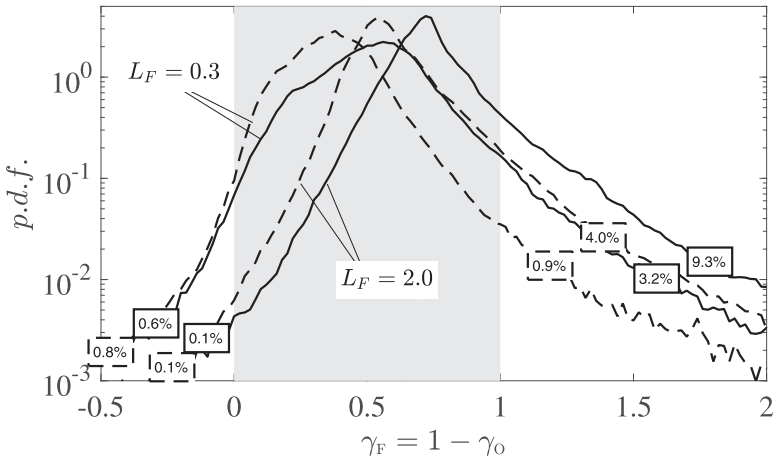

Fig. 6. The probability density distribution of γ_F for $S = 0.5$ (solid curves) and $S = 1.0$ (dashed curves).

imum a temperature on the oxidizer side is much more frequent, especially for $L_F = 2$.

6. Conclusions

Departures of Burke–Schumann diffusion-flame temperatures from stoichiometric adiabatic values, associated with fuel Lewis numbers L_F different from unity are quantified here, for the first time, for canonical one-dimensional flamelet problems, for flames wrapped by a line vortex, and for three-dimensional flames embedded in temporal turbulent mixing layers. More pronounced differential-diffusion effects are found for intermediate values of the stoichiometric mixture fraction $Z_S = 1/(S+1)$, corresponding to diluted fuel-feed configurations with air-to-fuel stoichiometric ratios $S \sim 1$. As seen in Fig. 1, for these diluted flames superadiabatic temperature increments of up to 30% can be achieved for $L_F = 0.3$, whereas subadiabatic decrements of up to 15 % can be found with $L_F = 2.0$. Unexpectedly, the resulting temperature departures can be larger than those predicted when reactant transport is exclusively governed by diffusion fluxes. When dependences of flame-temperature distributions on Peclet numbers and fuel-feed dilution are quantified for flames wrapped by a potential vortex, with results given in Figs. 2 and 3, reverse differential-diffusion effects are encountered near the vortex core for very diluted flames with $Z_S > 1/2$, leading to superadiabatic/subadiabatic temperatures for values of L_F larger/smaller than unity. Under those conditions, the peak temperature sometimes does not occur at the stoichiometric flame sheet. As revealed by direct numerical simulations, the unexpected features displayed by the vortex-flame model when $L_F \neq 1$ are also encountered in turbulent flames in time-evolving mixing layers, with associated probability density distributions shown in Figs. 5 and 6, thereby providing additional evidence for the nontrivial role of differential diffusion in nonpremixed–combustion systems.

The Burke-Schumann approximation provides the basic flow structure for flames when a strong temperature dependence of the fuel-oxidation rate confines the chemical reaction to thin layers. Variations of the resulting peak temperature resulting from differential-diffusion effects, computed here, modify the rate of fuel oxidation in these reaction layers [3]. Decreasing peak temperatures promote incomplete combustion, increasing fuel leakage, and may lead to local flame extinction, which would alter these overall flame structures. For example, this could arise in diluted hydrogen-air flames wrapped in a vortex, which display a rapid flame-temperature decrease with decreasing radial distances, seen in Fig. 3, so that extinction near the vortex core may occur.

Previous finite-rate computations of turbulent diffusion flames [5] have revealed that differential-diffusion effects diminish for increasing Reynolds numbers as a consequence of the combined effects of turbulent mixing and finite-rate chemistry. The effect of the former has been isolated in our work by employing the Burke–Schumann limit. Additional computations considering varying Reynolds numbers and including larger values of S corresponding to undiluted fuel feed could be useful in further assessing interactions of turbulent mixing and differential diffusion.

Acknowledgments

This work was supported by the US AFOSR Grant no. FA9550-16-1-0443. Computational resources were provided by the San Diego Su-

Please cite this article as: A. Almagro et al., Effects of differential diffusion on nonpremixed-flame temperature, Proceedings of the Combustion Institute (2018), https://doi.org/10.1016/j.proci.2018.06.176

percomputer Center through XSEDE award # CTS160006.

References

[1] R.W. Bilger, *Ann. Rev. Fluid Mech.* 21 (1989) 101–135.
[2] A. Liñán, M. Vera, A.L. Sánchez, *Ann. Rev. Fluid Mech.* 47 (2015) 293–314.
[3] A. Liñán, D. Martínez-Ruiz, M. Vera, A.L. Sánchez, *Combust. Flame* 175 (2017) 91–106.
[4] W.T. Ashurst, N. Peters, M. Smooke, *Combust. Sci. Technol.* 53 (1987) 339–375.
[5] C. Han, D.O. Lignell, E.R. Hawkes, J.H. Chen, H. Wang, *Int. J. Hydrogen Energy* 42 (2017) 11879–11892.
[6] F.A. Williams, *Combustion Theory*, Second ed., Benjamin Cummings, Menlo Park, CA., 1985.
[7] N. Peters, *Turbulent Combustion*, Cambridge University Press, 2000.
[8] F.E. Marble, in: Recent Advances in the Aerospace Sciences, Springer US, 1985, pp. pp.395–413.
[9] A.R. Karagozian, F.E. Marble, *Combust. Sci. Technol.* 45 (1986) 65–84.
[10] M. Alain, S.M. Candel, *Combust. Sci. Technol.* 60 (1988) 79–96.
[11] A. Liñán, in: Real Academia de Ciencias Exactas, Físicas y Naturales, Madrid, Spain, 1991, pp. 106–114.
[12] F.J. Higuera, R.D. Moser, Summer Program, Center for Turbulence Research, Stanford University, 1994, pp. 19–40.
[13] C. Pantano, S. Sarkar, F.A. Williams, *J. Fluid Mech* 481 (2003) 291–328.
[14] A. Liñán, P. Orlandi, R. Verzico, F.J. Higuera, Summer Program, Center for Turbulence Research, Stanford University, 1994, pp. 5–18.
[15] A. Almagro, M. García-Villalba, O. Flores, *J. Fluid Mech.* 830 (2017) 569–601.
[16] A. Almagro, *Direct Numerical Simulation of Reactive and Non-Reactive Mixing Layers*, Universidad Carlos III de Madrid, Spain, 2017 (Ph.d. thesis).

Please cite this article as: A. Almagro et al., Effects of differential diffusion on nonpremixed-flame temperature, Proceedings of the Combustion Institute (2018), https://doi.org/10.1016/j.proci.2018.06.176